L3 Note 2473
October 15, 1999

TWO-PHOTON COLLISIONS AT LEP [a]

M. N. KIENZLE-FOCACCI

Département de Physique Nucléaire et Corpusculaire, 24 quai Ernest-Ansermet, CH-1211 GENEVE 4, Switzerland

E-mail: maria.kienzle@cern.ch

Our knowledge of two-photon processes largely increased during the last years thanks to the large samples of $e^+e^- \rightarrow e^+e^-$hadrons events obtained at LEP. The two-photon total cross-sections are studied for real and for virtual photons by tagging the scattered electrons. Inclusive c-quark and b-quark production and the differential cross sections of jets and single particle production are a test of NLO perturbative QCD calculations. Two-photon resonance formation gives an insight on the internal structure of the mesons and provides a test for gluonium candidates.

1 Introduction

In recent years hadron production has been studied in a variety of channels in two-photon collisions at LEP (LEP1, $\sqrt{s} \simeq 91$ GeV, and LEP2, $\sqrt{s} > 160$ GeV). The integrated luminosity available to each of the four LEP experiments at the various energies is indicated in Fig.1. As illustrated in the figure, at LEP2, the two-photon interaction is the main source of hadronic events. It is therefore possible to increase our knowledge on the two-photon processes. This is highly desirable in order to test perturbative and non-perturbative QCD calculations and to better understand the background in new particles searches and at future e^+e^- colliders.

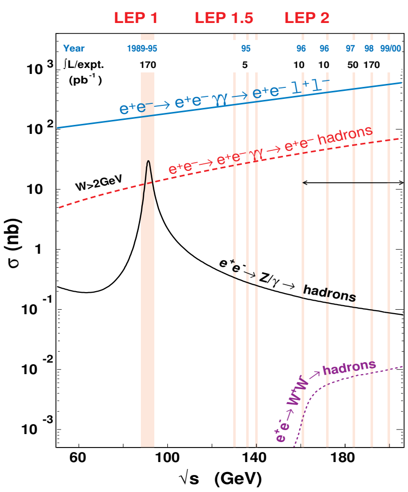

Figure 1: Cross-sections of the main hadronic channels as a function of the LEP energy. The vertical bands indicate the beam energies and the integrated luminosities for each year of data taking.

The Monte Carlo models play a central role in this study. Two generators, PHOJET [1] and PYTHIA [2], aim to a good description of the two-photon interactions. At the

[a] Talk given at EDS99, International Conference on Elasic and Diffractive Scattering (VIIIth "Blois Workshop") Protvino 1999.

present level of theoretical understanding, a perturbative QCD contribution is added to a non perturbative diffractive phenomenology. The interacting photon is considered as a superposition of a *bare* photon and an *hadronic* photon

$$| \gamma >= \sqrt{Z_3} \mid \gamma_{bare} > + \frac{e}{f_{q\bar{q}}} \mid q\bar{q} > + \frac{e}{f_{q\bar{q}^*}} \mid q\bar{q}^* > \qquad (1)$$

whith $Z_3 = 1 - (e/f_{q\bar{q}})^2 - (e/f_{q\bar{q}^*})^2$. The *bare* photon interacts in a point-like way. For the *hadronic* component it is assumed that the photon fluctuates into a $q\bar{q}$ pair which interacts hadronically. Due to the quantum numbers of the photon, it is expected that the $q\bar{q}$ pairs predominantly form particles with small masses like ρ, ω, ϕ vector mesons (VDM). The hadronic interactions are separated into hard ($q\bar{q}^*$) and soft interactions by a transverse momentum cutoff p_t^{cut}. The subprocesses involving transverse momenta greater than this scale can be calculated by perturbative QCD. The $\gamma^*\gamma^* \rightarrow$ *hadrons* cross section is therefore composed by a "soft" interaction, which can be described by hadronic phenomenology, like the Regge poles, a point-like two-photon reaction, $\gamma\gamma \rightarrow q\bar{q}$ (*direct* process), which is calculable in QED and an "hard component" which implies the knowledge of the quark and gluon distributions (pdf) inside the photon (*resolved* processes). In order to describe the data the models have to include *i*) a consistent transition between low p_t and high p_t events, *ii*) a description of elastic and diffractive reactions like $\gamma\gamma \rightarrow$ VV, *iii*) a description of the structure of the photon (pdf) and of the primordial k_T distribution of the partons inside the photon, *iiii*) a unitarization scheme for the cross sections. In the PHOJET model γp and pp data are used to fix the couplings of the Pomeron and of the Reggeon to the $q\bar{q}$ fluctuation of the photon. The cross sections are then calculated in the framework of a Dual Parton Model, with the unitarization constraint. The model [3] of Schuler and Sjöstrand, implemented in PYTHIA, aims to a smooth superposition of hadron-like and point-like photon interactions. In the following the predictions of the two models will be compared to the LEP results. The data will be also compared to QCD theoretical calculations.

2 Two-photon cross-sections

2.1 Total $\gamma\gamma$ cross-section

At LEP2 the dominant two-photon process $e^+e^- \rightarrow e^+e^-$ *hadrons* is easily separated from the annihilation channels (Fig.2). The analysis can be performed with a low background in a wide range of the two-photon center of mass energy, $W_{\gamma\gamma}$. The total cross-section of two real photons has been measured by L3 [4] and OPAL [5] in the range 5 GeV $< W_{\gamma\gamma} <$ 145 GeV. The value of $W_{\gamma\gamma}$ is

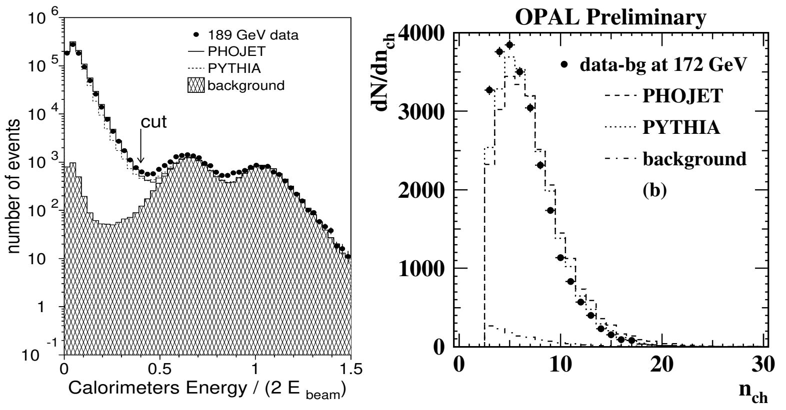

Figure 2: (left) Total energy in the electromagnetic and hadronic calorimeters of the L3 detector, normalised to the centre-of-mass energy. The two-photon events, below the cut, are selected with a low background from $e^+e^- \to e^+e^- \tau^+\tau^-$ and annihilation events. (right) Distribution of charged tracks compared to Monte Carlo predictions, for two-photon events selected by OPAL.

obtained from the effective mass of the measured hadrons, $W_{\rm vis}$, by unfolding the detector acceptance, which is rather poor in the diffractive region, near to the beam direction. The differential cross section $d\sigma/dW_{\gamma\gamma}$, as measured by L3 at different collision energies, is shown in Fig.3. The fast decrease of the cross section as a function of $W_{\gamma\gamma}$ is due to the two-photon luminosity function, $\mathcal{L}_{\gamma\gamma}$, which depends on $\tau = W^2_{\gamma\gamma}/s$. To extract the total cross section of two real photons the photon flux $\mathcal{L}_{\gamma\gamma}$ is calculated [6] and the cross section is extrapolated to $Q^2 = 0$ (Fig.3 right). The unfolding procedure introduces a strong bin-to-bin correlation which must be taken into account when comparing the data to different models. The two generators, employed to correct the data, PYTHIA and PHOJET, give a difference of ∼20% in the absolute scale of $\sigma_{\gamma\gamma}$. The measurements of L3 and OPAL agree if the same Monte Carlo is used (Fig.3 right). The two-photon cross-section shows the typical behaviour [7] of hadron-hadron total cross-sections: a fast decrease for $W_{\gamma\gamma} < 20$ GeV, due to reggeon exchange, and a slow increase at higher energies, described by a "soft" Pomeron. The rise of $\sigma_{\gamma\gamma}$ with $W_{\gamma\gamma}$ is faster than the one observed in hadron-hadron or γp cross-sections [8]; a simple factorisation ansatz [9] $\sigma_{\gamma\gamma} = \sigma^2_{\gamma p}/\sigma_{pp}$ is excluded (see the curve from Schuler and Sjöstrand [3] in Fig.3). A fit to the L3 data with the parametrisation $\sigma_{\gamma\gamma} = A \times W_{\gamma\gamma}^{2(\alpha_P(0)-1)}$, for $W_{\gamma\gamma} >$

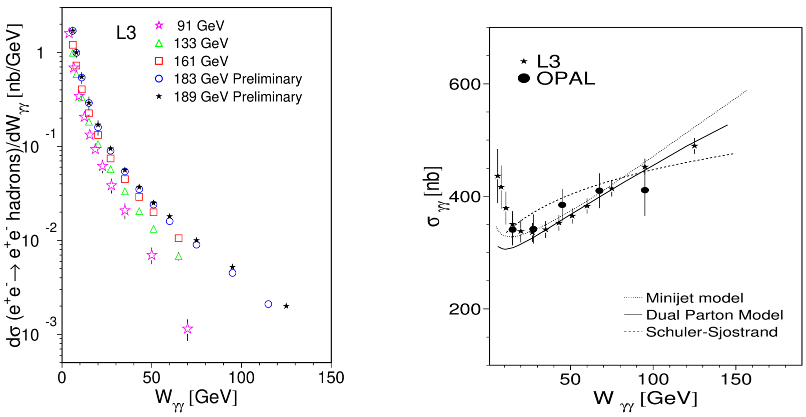

Figure 3: (left) The differential cross section $d\sigma/dW_{\gamma\gamma}$ measured at various beam energies. (right) Two-photon total cross-section as measured by L3 [4] and by OPAL [5], both unfolded with PHOJET. The minijet model [11] and the Dual Parton model [1] reproduce well the data, while the $W_{\gamma\gamma}$dependence predicted by Schuler and Sjöstrand [3] does not agree with the data.

40 GeV, gives a value $(\alpha_P(0) - 1) = 0.14 \pm 0.02$ [b] to be compared with the universal value[8] of 0.095 ± 0.002. Many theoretical predictions[10] exist , the rise of $\sigma_{\gamma\gamma}$ is rather well described by most of the models which take into account the direct coupling of the photon to $q\bar{q}$ as, for example, the minijet model[11].

2.2 Diffractive processes

The different values of $\sigma_{\gamma\gamma}$ obtained by correcting the data with PYTHIA and PHOJET may be related to the description of the diffractive component (Fig.4 left) for which the detectors acceptance is small. L3 has investigated the diffractive contribution by studying exclusive and inclusive ρ^0 production[4] (Fig.5). In the limited kinematical range accessible to the experiment, 3 GeV $< W_{\gamma\gamma} <$ 8 GeV, both generators fail to reproduce the data (Fig.4 right): PHOJET predicts too few ρ^0 events while the almost constant production in $W_{\gamma\gamma}$, predicted by PYTHIA, is not observed. More data are necessary to investigate these processes.

[b]The numerical value of $\alpha_P(0)$ depends on the parametrisation used for the fit and on the chosen $W_{\gamma\gamma}$ interval [4].

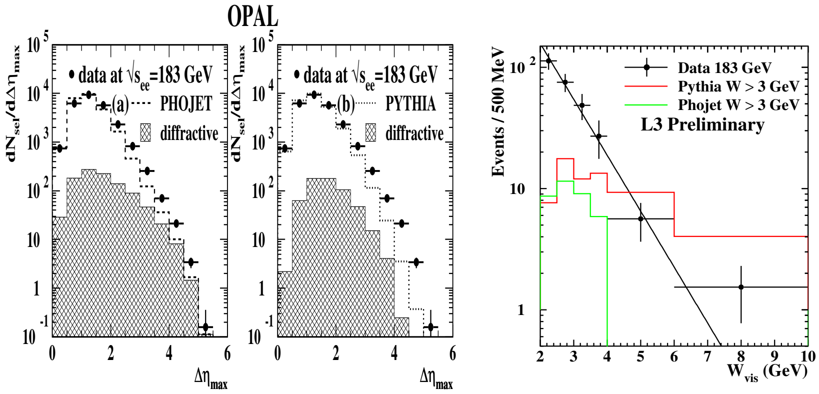

Figure 4: (left) The diffractive component, shown for the distribution of the maximum rapidity gap between any two hadrons, has a different shape in PYTHIA and PHOJET. (right) Number of $\gamma\gamma \to \rho^0 X$ events as a function of $W_{\rm vis}$ compared to PYTHIA and to PHOJET predictions, normalised to the luminosity of the data.

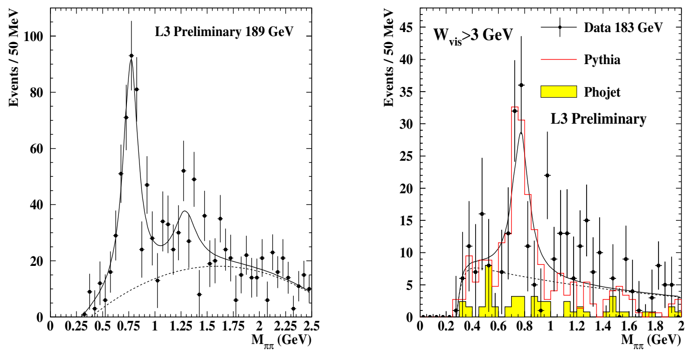

Figure 5: Effective mass of two oppositely charged pions, after subtraction of background estimated from the wrong sign combinations, for two-photon events with $W_{\rm vis} > 3$ GeV (left) in the exclusive channel $e^+e^- \to e^+e^-\pi^+\pi^-\pi^+\pi^-$ and (right) in inclusive $e^+e^- \to e^+e^-\rho^0$ production.

2.3 Double tag measurements

When both scattered electrons are detected, the $W_{\gamma\gamma}$ mass can be measured from the four-momenta of the two scattered electrons, thus strongly reducing the model dependence of the cross-section measurement. The cross-section of $\gamma^*\gamma^*$ collisions has been measured at LEP by L3 [12] and OPAL [13] in the range of $3\,\mathrm{GeV}^2 < \mathrm{Q}^2_{1,2} < 37\,\mathrm{GeV}^2$. Since the two photons are highly virtual and, unlike the proton, they do not contain constituent quarks with an unknown density distribution, one may hope to have a complete perturbative QCD calculation under particular kinematical conditions. A recent QCD approach is based on

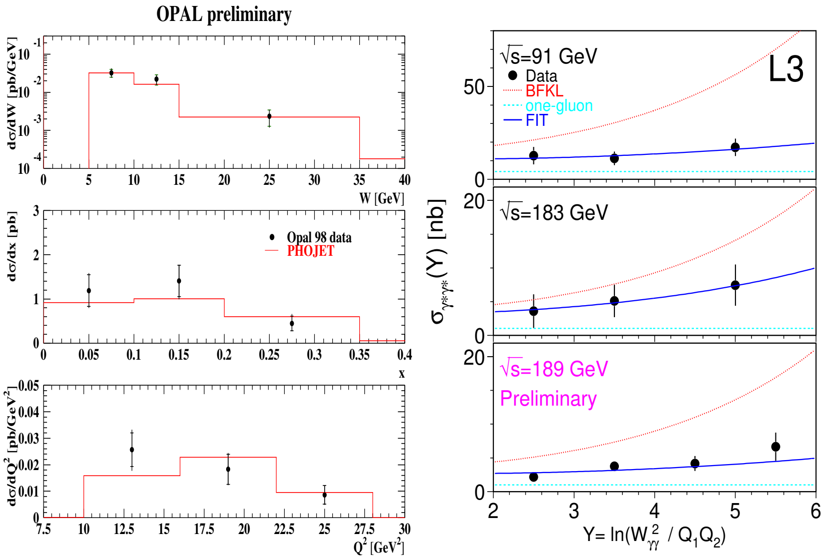

Figure 6: (left) The differential cross-section of double tag events compared to PHOJET Monte Carlo predictions [13] and (right) the two photon cross-sections at LEP1 and LEP2 compared to LO-BFKL calculations after subtraction of the direct contribution [12].

the BFKL equation [14]. The $\gamma^*\gamma^*$ interaction is described as the interaction of two $q\bar{q}$ pairs scattering off each other via multiple gluon exchange. In this scheme the cross-section for the collision of two virtual photons [15,16] depends upon the "hard Pomeron" intercept $\alpha_P - 1 = 0.53$, at the LO, whereas in NLO the BFKL contribution is calculated to be smaller, $\alpha_P - 1 \simeq 0.17$ [17]. The results from L3 and OPAL (Fig.6) are well described by PHOJET, which uses the GRV-LO parton density [18] in the photon and leading order perturbative QCD. The LO BFKL calculations, shown in Fig.6 (right) with dotted lines, are too high. By leaving α_P as a free parameter in the LO formula [15] , a combined fit to the L3 data gives a value of $\alpha_P - 1 = 0.29 \pm 0.025$ with χ^2/d.o.f =7/9.

2.4 Inclusive c and b production

Inclusive heavy quark production is well suited to study hard interactions, the high mass of the quark providing a natural hard scale for perturbative QCD calculations [19].

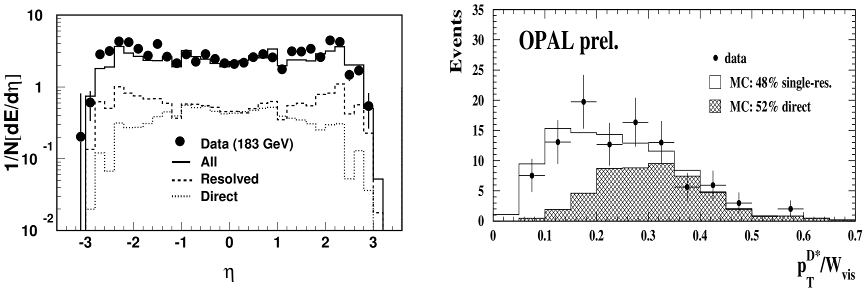

Figure 7: (left) The rapidity distribution of hadrons in events with an electron identifying the heavy-quark semileptonic decay. The data are compared to PYTHIA predictions. (right) The p_T distribution of the D^* normalised to the visible mass of the event. Both direct and resolved contributions are necessary to reproduce the shape of the data.

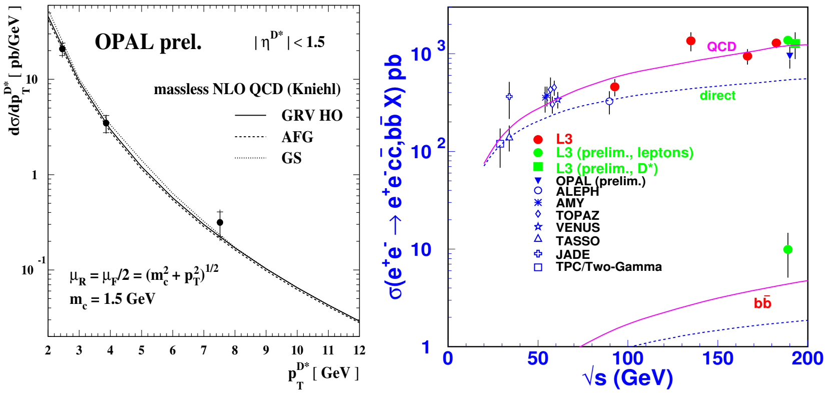

Figure 8: (left) The differential cross-section for inclusive D^* production, compared to NLO QCD calculations [22]. (right) The cross-section for heavy quarks production as measured at LEP and at previous e^+e^- colliders.

At LEP2 energies the direct and resolved processes contribute equally to the cross-section. The resolved contribution is dominated by quark-gluon fusion, γg $\rightarrow q\bar{q}$, thus this measurement provides a strong constraint for the determination of the gluon content in the photon. L3 [20] tags the presence of a charm-quark by identifying a lepton (electron or muon) in the event or by recostructing a $D^*\rightarrow D^0\pi$ in the decay chain $D^0\rightarrow K^-\pi^+$ and $D^0\rightarrow K^-\pi^+\pi^0$. OPAL [21] tags the charm-quark with $D^*\rightarrow D^0\pi$, $D^0\rightarrow K^-\pi^+$ and $D^0\rightarrow K^-\pi^+\pi^-\pi^+$. The rapidity distribution of the hadrons in events selected with an electron [20], to identify the charm semileptonic decay, is well reproduced by PYTHIA (Fig.7 left) including direct and resolved processes. A good separation of the two contributions is obtained by OPAL by associating the D^* to a dijet analysis or by inspection of the p_t distribution of the D^* (Fig.7 right). The differential D^* cross section (Fig.8 left), measured inside the kinematical range of the detector acceptance, is almost independent on the Monte Carlo models used for efficiency corrections. It agrees well with NLO calculations [22]. The dependence on the pdf's, on the factorisation and renormalisation scales is small. With a stronger model dependence the data are extrapolated to the total charm production cross-section (Fig.8 right). The rise of the cross-section above the charm threshold and the importance of a full QCD calculation [19] are well demonstrated by the LEP data. The calculations depend on the charm mass, which can be determined once more data is available. In Fig.8 (right) also the b production cross-section is shown, as it has been measured for the first time by L3 [20], by tagging the b-quark with high p_t leptons.

3 Jets and single particle production

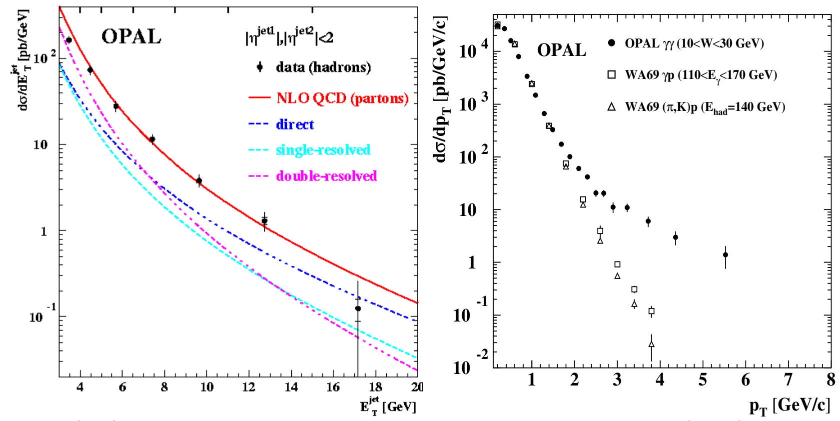

Figure 9: (left) Differential cross-section as a function of E_T for jets and (right) as a function of p_t for charged hadron production [23]. The p_t spectrum is harder in $\gamma\gamma$ than in γp and (π,K)p interactions.

Until now only OPAL[23] published measurements of high p_t jets and inclusive charged hadron and K^0_S production. The jet and inclusive single-particle differential cross sections agree well with NLO calculations[24], using GRV[18] pdf (Fig.9 left). All processes are necessary: the direct contribution is dominant at high p_t, the double-resolved processes (ex.: gg $\rightarrow$ gg) are necessary at low p_t values.

It is also interesting to compare the p_t distribution of charged hadron produced by different interactions ($\gamma\gamma$, γp and πp) (Fig.9 right). While the p_t spectrum of hadrons in photoproduction is similar to the one observed in pure hadronic interactions, the spectrum measured in two-photon interactions is harder due to the point-like photon coupling. OPAL notices also that PHOJET and PYTHIA both underestimate the K^0_S production by $\simeq$ 30 %. For dijet events the x_γ [c] distribution separates the direct from resolved processes. The angular distribution in the dijet center-of-mass shows a clear difference between the direct process, where a quark is exchanged in the t-channel and the double-resolved processes, dominated by gluon exchange (Fig.10).

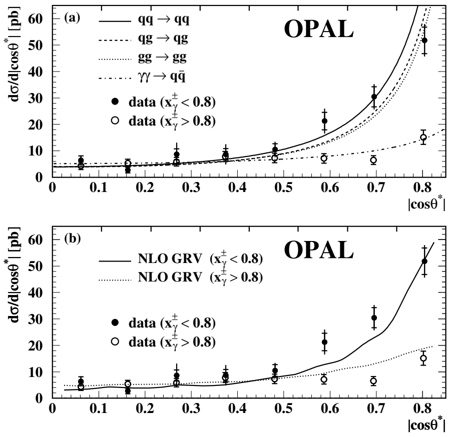

Figure 10: The angular distribution in the dijet center-of-mass system for *direct* ($x_\gamma >$ 0.8) and *double-resolved* ($x_\gamma <$ 0.8) events[23].

4 Resonance formation

Resonance formation in $\gamma\gamma$ interactions offers a clean experimental environment to study the spectrum of $q\bar{q}$ bound states. Only C=+1 states can be formed and the spin-parity quantum numbers are limited by the two-photon initial state. The measurement of the two-photon width, $\Gamma_{\gamma\gamma}$, and of the meson form factor, $F(Q^2)$, give an insight on the charge and the wave function of the valence quarks. The presence of a gluon component can be tested and pure glueball states are expected to have a two-photon width much smaller than $q\bar{q}$ states. For heavy quarks, $c\bar{c}$ states, a measurement of α_s is possible by

[c] The variable x_γ measures the momentum of the interacting particle, relative to the photon momentum, x_γ= 1 for a direct process, x_γ< 1 for a resolved process.

comparing two-photon to two-gluon partial widths. At LEP many exclusive channels are studied as shown in Table 1.

4.1 The $\eta^{'}(958)$ *form factor and the recurrence of* $a_2(1320)$

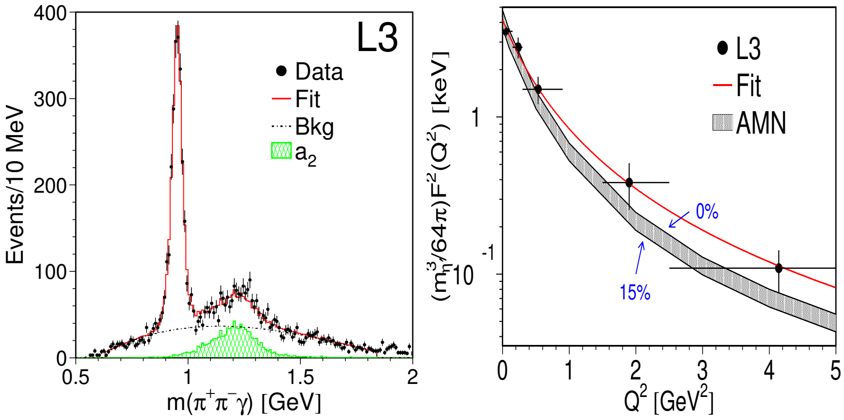

Figure 11: (left) The $\pi^+\pi^-\gamma$ mass spectrum for data [25] at $\sqrt{s}$=91 GeV. (right) Measured form factor fitted by a VDM pole form and compared to QCD predictions [34].

The $\pi^+\pi^-\gamma$ spectrum (Fig.11) is dominated by the peak of the $\eta'(958)$ resonance, the nearby enhancement is due to the a_2 (1320) $\to \pi^+\pi^-\pi^0$, when a photon of the π^0 decay goes undetected. For this spectrum the events with small transverse momentum, $|\overrightarrow{p_t}(\pi^+\pi^-\gamma)|^2 \leq 0.01$ GeV^2, are selected. These events allow an accurate measurement of the two-photon width (Table 1). The $e^+e^- \to e^+e^-\eta'$ cross-section is also measured as a function of Q^2, by using the relation $|\overrightarrow{p_t}(\pi^+\pi^-\gamma)|^2 = Q^2$ and the tagged events. The η' form factor thus obtained is well reproduced by the vector dominance form $F(Q^2)= [1/(1 + Q^2/\Lambda^2)]$. A fit to the data (Fig.11 right) gives a pole mass value $\Lambda = 900 \pm 46$ (stat.) ± 22 (sys.) MeV, consistent with the VDM prediction [33] of $\Lambda = 830$ MeV. Anisovich, Melikhov and Nikonov [34] describe the perturbative and non-perturbative QCD regions with few parameters. Their predictions are indicated as a shaded area in Fig.11, ranging from no gluonium content (upper line) to 15% gluonium content (lower line). No definite conclusion can be derived from the comparison to the data, since the theoretical Q^2 dependence is somewhat different from the one observed. The perturbative QCD calculations of Jacob, Kroll and Raulfs [35] agree with the experimental measurement for $Q^2 \geq 2$ GeV^2.

The $\pi^+\pi^-\pi^0$ spectrum is dominated by the a_2 (1320) resonance [26]. The spin-parity analysis of the $\rho\pi$ and $f_2\pi$ channels shows evidence of a wide, 2^{++} state with M=1752±21 MeV and Γ=150±110 MeV. This observation confirms the result of a partial wave analysis of the $\pi^+\pi^-\pi^-$ system performed on data obtained at the Serpukhov accelerator [36]. This state can be interpreted as a radial excitation of the a_2 (1320) [37].

4.2 The $K^0_s K\pi$ channel

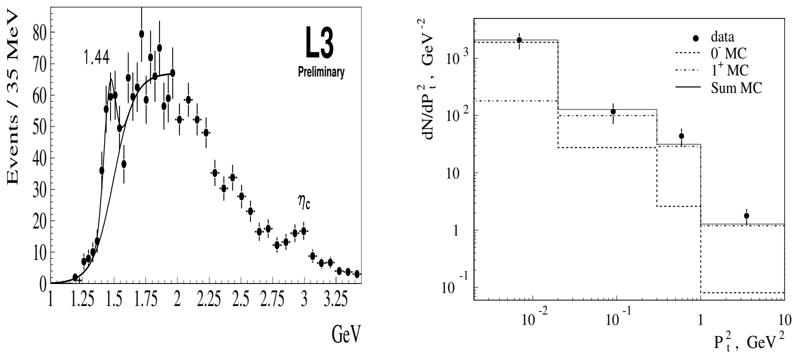

Figure 12: (left) The $K^0_S K^\pm\pi^\mp$ spectrum [27]. (right) The $|\overrightarrow{pt}|^2 \simeq Q^2$ distribution for the peak at ~1440 MeV. The maximum likelihood fit (solid line) is the sum of the $J^P = 0^-$ (dotted line) and the $J^P = 1^+$ (dash-dotted line) components.

The reaction $\gamma\gamma \to K^0_S K^\pm\pi^\mp$ is studied by L3 [27] with the full available statistics, for a total integrated luminosity of 250 pb^{-1}. In this channel, a part from the η_c (2980) peak, there is a peak at threshold containing 119 ± 22 events (Fig.12). A gaussian fit gives the values of M=1465±31 MeV and σ=45±5 MeV, the experimental resolution being 24 MeV. The evolution of this signal with Q^2 (Fig.12 right) is studied with the same method used for the η' form factor. The data cannot be explained by a pure spin-parity state. A confidence level smaller than 1% is obtained for both pure $J^P = 0^-$ and pure $J^P = 1^+$ hypotheses, simulated by Monte Carlo. A fit using a combination of the two waves gives a confidence level of 50% , 49±1 events for the 0^- state, identified with the η (1440), and 63±6 events for the 1^+ state, called f_1 (1450). The two photon width of the η (1440) is determined using events with $|\overrightarrow{pt}(K^0_S K^\pm\pi^\mp)|^2 \leq 0.05$ GeV^2, where the 0^- state clearly dominates. Comparing the two-photon width (table 1) to the total width of

η (1440) [8], a value of 9.5 $\pm$ 3.0 is obtained for the stickiness [38]. This value is similar to the ones obtained for ordinary mesons showing no evidence for a glueball nature of the η (1440).

4.3 $\mathrm{K_s^0K_s^0}$ *resonances and glueball search*

The $\mathrm{K}_s^0\mathrm{K}_s^0$ mass spectrum [27], Fig.13, shows clear evidence for the formation of the $f_2^{'}(1525)$ tensor meson. A Breit-Wigner fit gives 184$\pm$ 27 events, M=1523$\pm$8 MeV and Γ =89$\pm$37 MeV. Around 1300 MeV, $f_2(1270)-a_2(1320)$ destructive interference is observed consistent with theoretical predictions [39]. In addition, there is an enhancement of 171$\pm$26 events at M=1765$\pm$22 MeV and Γ =200$\pm$50 MeV which is possibly due to the formation of a radially excited state of the $f_2^{'}$ [37]. A study of the angular distribution of the $\mathrm{K_S^0}$ in the two-photon centre-of-mass is in progress.

A search for the glueball candidate $\xi(2230)$ has been performed, motivated by the observation of a narrow peak [40] produced in radiative J/ψ decay. The absence of a signal in the $\mathrm{K}_s^0\mathrm{K}_s^0$ spectrum gives an upper limit for the two-photon width of 1.5 eV at 95% CL, under the hypothesis of a pure spin 2, helicity 2 state. This low value and a stickiness [38] greater than 68 are inconsistent with a $q\bar{q}$ content, a glueball hypothesis for the $\xi(2230)$ is strongly favoured, if this state exists.

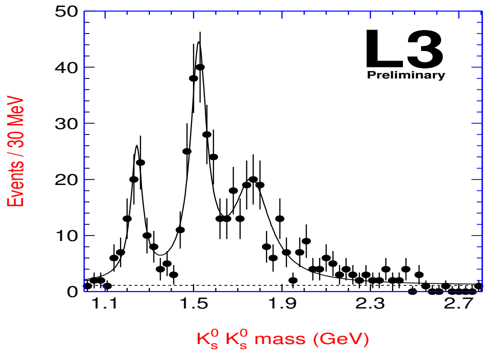

Figure 13: The $\mathrm{K}_s^0\mathrm{K}_s^0$ mass spectrum.

4.4 Charmonium Production

The individual η_c (2980) decay channels have branching ratios of the order of 1-2 %. As a consequence many decay channels have to be analysed and the two-photon width accuracy is limited by the poor knowledge of the η_c branching ratios [8]. Using LEP I and LEP II data, with a total luminosity of 193 pb^{-1} , L3 [30] measures the η_c (2980) two-photon width (table 1), by combining the events of nine different decay modes. Fig.14 shows the mass distribution of selected events with one of the scattered electron detected in the forward calorimeters. These events allow the measurement of the η_c transition form factor in two Q^2 bins, (0.2 GeV^2 < Q^2 < 9 GeV^2). The η_c form-factor measurement is

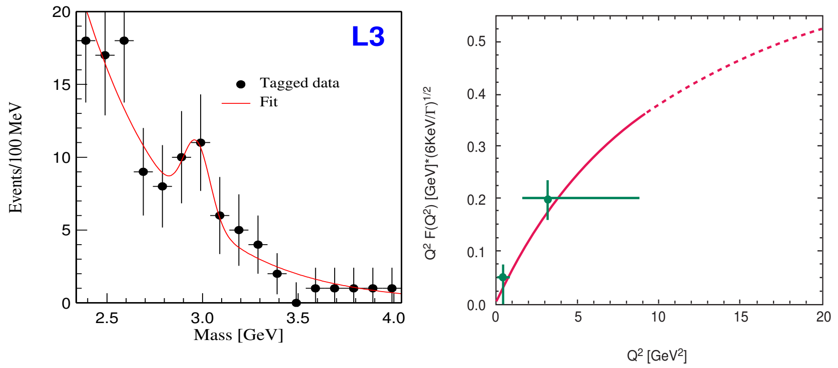

Figure 14: (left) The η_c (2980) signal for single-tag events [30]. (right) The measured η_c form-factor compared to QCD calculations [41].

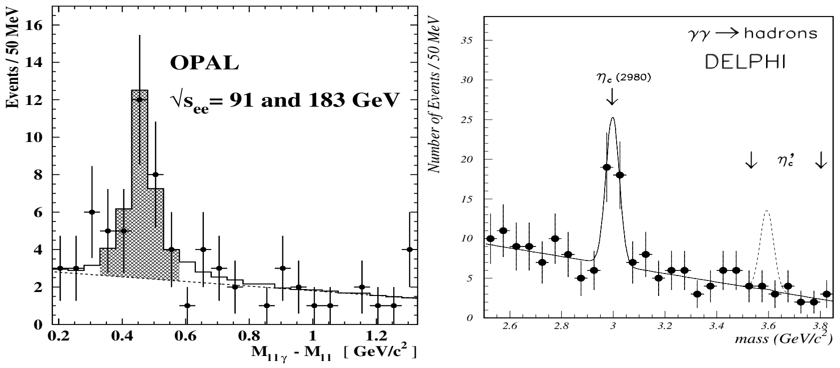

Figure 15: (left) The $\chi_{c2}(3550)$ signal as measured by OPAL [31]. (right) The η_c (2980) signal and the search for η_c'.

consistent with a J/ψ pole in the VDM parametrisation and is in agreement with theoretical calculations [41].

The $\chi_{c2}(3550)$ is detected [31,32] through its dominant radiative decay to J/ψ: $\chi_{c2} \rightarrow \gamma$ J/$\psi \rightarrow \gamma e^+e^-$, $\gamma\mu^+\mu^-$ (Fig.15 left). While the two-photon width of the η_c is well in agreement with the value measured in $p\bar{p} \rightarrow \gamma\gamma$ [42] annihilation , for the χ_{c2} a discrepancy of ~ 3 standard deviations is observed. The combined two-photon results is $\Gamma_{\gamma\gamma}(\chi_{c2}) = 1.23 \pm 0.23$ keV and the new $p\bar{p}$ measurement of E835 [44], $\Gamma_{\gamma\gamma}= 0.31 \pm 0.05 \pm 0.04$ keV confirms the previous E760 measurement [43].

No η_c' signal is observed neither at LEP, where DELPHI [45] (Figure 14) and L3 [30] searched for it, nor in $p\bar{p}$ annihilation [42].

Table 1: The resonances studied at LEP

Resonance	Final state	J^{PC}	$\Gamma_{\gamma\gamma}$ (keV)
η' (958)	$\pi^+\pi^-\gamma$	0^{-+}	$4.17 \pm 0.10 \pm 0.27$ [25]
a_2 (1320)	$\pi^+\pi^-\pi^0$	2^{++}	$0.98 \pm 0.05 \pm 0.09$ [26]
a_2' (1750)	$\pi^+\pi^-\pi^0$	2^{++}	$0.29 \pm 0.04 \pm 0.02/(BR)$ [26]
η (1440)	$K^0_s K\pi$	0^{-+}	$0.17 \pm 0.05/(BR)$ [27]
f_1 (1450)	$K^0_s K\pi$	1^{++}	Ref. [27]
f_2' (1525)	$K^0_s K^0_s$	2^{++}	$0.09 \pm 0.02 \pm 0.02/(BR)$ [28]
X (1750)	$K^0_s K^0_s$	0 or 2	Ref. [27]
η_c (2980)	12 Channels	0^{-+}	$8.0 \pm 2.3 \pm 2.4$ [29]
η_c (2980)	9 Channels	0^{-+}	$6.9 \pm 1.9 \pm 2.0$ [30]
χ_{c2}(3555)	$J/\psi\ \gamma$	2^{++}	$1.76 \pm 0.47 \pm 0.40$ [31]
χ_{c2}(3555)	$J/\psi\ \gamma$	2^{++}	$1.02 \pm 0.40 \pm 0.17$ [32]

Conclusions and outlook

Our knowledge of two-photon physics has significantly increased with the analysis of LEP data. With a total integrated luminosity of ≥ 500 pb^{-1} at the end of LEP data taking, we expect a good sensitivity also to low cross-section channels. An improvement on our understanding of perturbative and non-perturbative QCD phenomena is possible, if the Monte Carlo models are carefully studied in order to better reproduce the experimental distributions of the two-photon events.

References

1. R. Engel, *Z. Phys.* C **66**, 203 (1995) ;
   R. Engel and J. Ranft, *Phys. Rev.* D **54**, 4246 (1996).
2. T. Sjöstrand, *Comput. Phys. Commun.* **82**, 74 (1994).
3. G.A. Schuler and T. Sjöstrand, *Z. Phys.* C **73**, 677 (1997).
4. L3 Coll., M. Acciari et al.,*Phys. Lett.* B **408**, 450 (1997);
   L3 Coll., M. Acciari et al., Submitted to EPS, Tampere, 1999.
5. OPAL Coll., G. Abbiendi et al., hep-ex/9906041 to appear in *Eur. Phys. J.*
6. V.M. Budnev, I.F. Ginzburg, G.V. Meledin and V.G. Serbo, *Phys. Rep.* C **15**, 181 (1974);
   G.A. Schuler, *Comput. Phys. Commun.* **108**, 279 (1998).
7. A. Donnachie and P. V. Landshoff, *Phys. Lett.* B **296**, 227 (1992).
8. Review of Particle Physics, *Eur. Phys. J* **3**, 205 (1998).
9. V.N.Gribov and I.Ya.Pomeranchuk, *Phys. Rev. Lett.* **8**, 343 (1962).
   S.J.Brodsky, *J.Phys.Suppl. (Paris)* 35 1974 C2-69.
   K.V.L.Sarma and V. Singh , *Phys. Lett.* B **101**, 201 (1981)
   C. Bourrely, J. Soffer, T.T. Wu, hep-ph/9903438.
10. A. Donnachie, H.G. Dosch and M. Rueter hep-ph/9810206 ;
    P. Desgrolard, M. Giffon, E. Martynov and E. Predazzi hep-ph/9811393
    B. Badelek, J. Kwiecinski and A.M. Stasto hep-ph/9903248 .
11. A. Corsetti, R.M.Godbole and G.Pancheri, *Phys. Lett.* B **435**, 441 (1998);
    R.M.Godbole and G.Pancheri, hep-ph/9903331.
12. L3 Coll., M. Acciarri et al., *Phys. Lett.* B **453**, 333 (1999);
    L3 Coll., M. Acciarri et al., Submitted to EPS, Tampere, 1999.
13. OPAL Coll., G. Abbiendi et al. , Submitted to EPS, Tampere, 1999.
14. E.A. Kuraev, L.N. Lipatov and V.S. Fadin, Sov. Phys. JETP **45** (1977) 199;
    Ya.Ya. Balitski and L.N. Lipatov, Sov. J. Nucl. Phys. **28** (1978)822.
15. S.J. Brodsky, F. Hautmann and D.E. Soper, *Phys. Rev.* D **56**, 6957 (1997).
16. J. Bartels, A. De Roeck and H. Lotter, *Phys. Lett.* B **389**, 742 (1996);
    J. Bartels, A. De Roeck, C. Ewerz and H. Lotter, hep-ph/9710500.
17. S.J. Brodsky, V.S. Fadin, V.T. Kim, L.N. Lipatov and G.B. Pivovarov, hep-ph/99101229.
18. M. Glück, E. Reya and A. Vogt,*Phys. Rev.* D **46**, 1973 (1992)
19. M. Drees, M. Kramer, J. Zunft and P.M. Zerwas, *Phys. Lett.* B **306**, 371 (1993)

20. L3 Coll., M. Acciarri et al.,*Phys. Lett.* B **453**, 83 (1999);
L3 Coll., M. Acciarri et al., Submitted to EPS, Tampere, 1999 ;
L3 Coll., M. Acciarri et al., hep-ex/9909005 to appear in *Phys. Lett.* B.
21. OPAL Coll., G. Abbiendi et al. , Submitted to EPS, Tampere, 1999
22. J. Binnewies, B.A. Kniehl and G. Kramer, *Phys. Rev.* D **53**, 6110 (1996);
J. Binnewies, B.A. Kniehl and G. Kramer, *Phys. Rev.* D **58**, 014014 (1998).
23. OPAL Coll., K. Ackerstaff et al. , *Z. Phys.* C **73**, 433 (1997);
OPAL Coll., K. Ackerstaff et al. , *Eur. Phys. J* **C 6**, 253 (1999)
24. T.Kleinwort and G. Kramer, *Phys. Lett.* B **370**, 141 (1996).
25. L3 Coll., M. Acciarri et al., *Phys. Lett.* B **418**, 399 (1998).
26. L3 Coll., M. Acciarri et al., *Phys. Lett.* B **413**, 147 (1997).
27. L3 Coll., O. Adriani et al., Submitted to EPS, Tampere, 1999.
28. L3 Coll., M. Acciarri et al., *Phys. Lett.* B **363**, 118 (1995).
29. L3 Coll., O. Adriani et al., *Phys. Lett.* B **286**, 403 (1992).
30. L3 Coll., O. Adriani et al., *Phys. Lett.* B **461**, 155 (1999).
31. OPAL Coll.,K. Ackerstaff et al., *Phys. Lett.* B **439**, 197 (1998).
32. L3 Coll., M. Acciarri et al., *Phys. Lett.* B **453**, 73 (1999).
33. Ll. Ametler, J.Bijnens, A.Bramon, F.Cornet, *Phys. Rev.* D **45**, 986 (1992).
34. V.V.Anisovich, D.I.Melikhov and V.A.Nikonov, *Phys. Rev.* D **55**, 2918 (1997).
35. R.Jacob, P.Kroll and M.Raulfs, *J. Phys. G* **22**, 45 (1996).
36. Yu.M. Antipov et al., *Nucl. Phys.* B **63**, 153 (1973).
37. C. R. Münz, *Nucl. Phys.* A **609**, 364 (1996).
38. M. Chanowitz in Proceedings of the VIth International Workshop on Photon-Photon Collisions, World Scientific, 1984.
39. H. J. Lipkin, *Nucl. Phys.* B **7**, 321 (1968).
40. BES Collab., J. Z. Bai et al., *Phys. Rev. Lett.* **76**, 3502 (1996) ;
Mark III Collab., R. M. Baltrusaitis et al., *Phys. Rev. Lett.* **56**, 107 (1986).
41. T. Feldmann and P. Kroll, *Phys. Lett.* B **413**, 410 (1997).
42. E760 Coll., T.A. Armstrong et al., *Phys. Rev.* D **52**, 4839 (1995).
43. E760 Coll., T.A. Armstrong et al., *Phys. Rev. Lett.* **70**, 2988 (1993).
44. E835 Coll. represented by M. Stancari in PHOTON99, Proceedings to appear in *Nucl. Phys.* B.
45. DELPHI Coll., P. Abreu et al., *Phys. Lett.* B **441**, 479 (1998).